Electrically tunable organic vertical-cavity surface-emitting laser

Cite as: Appl. Phys. Lett. **105**, 073303 (2014); https://doi.org/10.1063/1.4893758
Submitted: 02 June 2014 . Accepted: 09 August 2014 . Published Online: 22 August 2014

Wendi Chang, Annie Wang, Apoorva Murarka, Gleb M. Akselrod, Corinne Packard, Jeffrey H. Lang, and Vladimir Bulović

Electrically tunable organic vertical-cavity surface-emitting laser

Wendi Chang,[a] Annie Wang,[a] Apoorva Murarka,[a] Gleb M. Akselrod,[b] Corinne Packard,[c] Jeffrey H. Lang, and Vladimir Bulović[d]
Department of Electrical Engineering and Computer Science, Massachusetts Institute of Technology, Cambridge, Massachusetts 02139, USA

(Received 2 June 2014; accepted 9 August 2014; published online 22 August 2014)

An electrically tunable organic vertical-cavity surface-emitting laser (VCSEL) is demonstrated and characterized. A lasing wavelength tunability of $\Delta\lambda = 10$ nm with 6 V actuation is shown for a red laser emission tuned between $\lambda = 637$ nm and $\lambda = 628$ nm. Wavelength tuning of the VCSEL structure is enabled by electrostatic deflection of a reflective flexible membrane that is suspended over an air gap and a dielectric mirror, forming a 3λ lasing cavity. The lasing gain medium consists of an evaporated organic thin film coated on a reflective membrane, which is then additively placed over a patterned substrate containing the dielectric mirror to fabricate an array of air-gap-VCSEL structures, each 100 μm in diameter. Beyond the electrostatic actuation of these tunable lasers, the VCSEL array geometry also has the potential to be used as pressure sensors with an all-optical remote excitation and readout and a pressure sensitivity of 64 Pa/nm in the demonstrated configuration. © *2014 AIP Publishing LLC*. [http://dx.doi.org/10.1063/1.4893758]

Development of compact, tunable laser arrays would benefit many applications including remote sensing, spectroscopy, optical switching, and large-area sensory skins. For applications that require large-area sensing, in particular, it is desirable to develop lasing structures that could be scalably deployed, and that operate in the visible or near-infrared range, which can be easily imaged. In this spectral range, molecular and polymeric organic thin films have already been demonstrated as broadly tunable lasing gain media,[1–3] with some reports demonstrating lasing over a >100 nm wavelength range using a single organic guest-host material system.[4] Also, due to the development of commercialized organic light emitting diode (OLED) technologies, multiple techniques have been developed for large-area deposition of organic thin films, such as those needed for demonstrating lasing action. In this work, we combine the large area-processability of organic thin films and a unique method for fabricating micro-electro-mechanical systems (MEMS) structures[5] to demonstrate arrays of organic vertical cavity surface-emitting lasers (VCSELs).[6] These devices have an effective cavity length that is as small as 3λ (3 wavelengths) and a lasing wavelength that is mechanically tunable over $\Delta\lambda = 10$ nm with 6 V of electrostatic membrane actuation.

Many earlier studies demonstrated lasing emission from organic thin films with a broad gain spectrum, which enabled broad tunability of the lasing emission line.[1–3] However, the lasing emission spectrum of a typical tunable organic solid-state laser, reported to date, is fixed by the fabrication process parameters and cannot be dynamically varied post-fabrication. In a few works that demonstrated dynamically tunable organic lasers, spectral tuning was implemented by using external mirror stages or with manually switchable gain media modules.[7,8] More compact, integrated organic lasing systems employing electroactive polymers or liquid crystals to electrically tune the emission wavelength have also been demonstrated, but often required high actuation voltages (0.1–3.5 kV).[9,10] In contrast, inorganic state-of-the-art lithographically fabricated air-gap MEMS VCSELs with epitaxially grown III-V gain medium have been shown with tunable spectral emission at much lower actuation voltages.[11] However, these VCSELs lase in the infra-red part of the spectrum, and are limited in scalability due to the size of the single-crystal wafers on which lasers are fabricated. Nevertheless, the key advantage of the lower operating voltage of these VCSELs is enabled by the lithographic fabrication processes that define the small physical dimensions of these structures, which can lead to large electric fields (and hence sufficient electromechanical force) even at small applied voltages. Thus, in this work we considered similar high-resolution schemes for fabricating organic VCSELs, but with the challenge of avoiding the organic film exposure to solvents and elevated temperatures, which can both deleteriously affect the organic gain materials.[12]

We fabricate integrated organic air-gap MEMS by using an additive solvent-free membrane transfer technique previously reported,[5] and which can be applied to fabrication of scalable, large area device arrays. Unlike the related tunable VCSEL-like structures reported previously,[13] our suspended membrane-cavity structure can be actuated electrically as well as mechanically and thus could potentially be employed as a contactless-readout pressure sensor.

Figure 1(a) shows a schematic cross-section of a completed array of devices. The lasing resonator of the VCSEL structure is formed by the vertical cavity between a bottom planar distributed Bragg reflector (DBR) and a movable silver mirror layer, which is part of the composite top membrane. A 500 nm-thick layer of tris-(8-hydroxyquinoline)aluminum (Alq_3) doped with 4–(dicyanomethylene)–2-methyl-6–(4-dimethylaminostyryl)–4H-pyran (DCM) is employed as the organic gain medium inside the resonator.[14] Upon

[a]W. Chang, A. Wang, and A. Murarka contributed equally to this work.
[b]Current address: Department of Electrical and Computer Engineering, Duke University, Durham, North Carolina 27708, USA.
[c]Current address: Department of Metallurgical and Materials Engineering, Colorado School of Mines, Golden, Colorado 80401, USA.
[d]bulovic@mit.edu

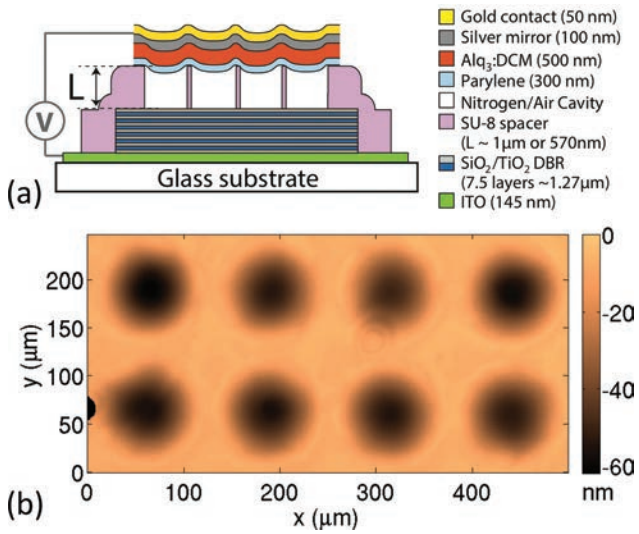

FIG. 1. (a) Schematic cross-section of tunable laser device structure. (b) Optical interferometry difference image of membrane-covered cavities under 20 V applied bias compared to 0 V, showing deflection of nearly 60 nm in the center of each cavity. The top-view contour image shows the suspended membranes deflecting into the underlying 100 μm-diameter cavities.

photoexcitation, excitons are generated inside the Alq_3 host and can undergo the Förster resonant energy transfer (FRET) to the DCM dopant molecules where they recombine to produce luminescence. The DCM molecules have a broad visible photoluminescence (gain) spectrum ranging 100 nm in wavelength, thus enabling a broad tunable range of the resulting VCSEL structure.

The device is fabricated on a glass substrate coated with a 150 nm-thick indium tin oxide (ITO) layer that serves as a bottom electrode. Alternating layers of silicon dioxide (SiO_2) and titanium dioxide (TiO_2) are sputter-deposited on top of ITO to form a distributed Bragg reflector (DBR) mirror with a 100 nm stop-band centered at $\lambda = 620$ nm, matching the peak photoluminescence (PL) emission of the organic gain medium. An SU-8 photoresist spacer layer, which in one set of devices is 1 μm thick and in the second set of devices is 570 nm thick, is then deposited and circular cavities 100 μm in diameter are patterned in it.

The top membrane is fabricated separately on a glass carrier substrate, starting with a 300 nm-thick structural support layer of parylene-C, which is chemically vapor-deposited on the glass. On top of this parylene-C polymer membrane, a thermally evaporated stack of 500 nm-thick layer of Alq_3:DCM (2.5% DCM doping) gain medium, 100 nm-thick silver mirror, and 50 nm-thick gold contact electrode are deposited in sequence. The completed membrane is attached to a flexible handle frame and mechanically delaminated from the glass. Supported only at the perimeter by the handle frame, the released composite membrane is then transferred in nitrogen atmosphere on top of the patterned SU-8 cavities to form suspended membrane cavities. Finally, the handle frame is removed, completing device fabrication.

Membrane deflection under electrostatic actuation was confirmed via optical interferometry (Wyko NT9100, Bruker Nano Inc.). The contour image in Figure 1(b) shows the deflection of the suspended membrane into the underlying $L = 1$ μm deep cavities when a 20 V bias is applied between the top gold contact and the bottom ITO electrode. Increasing the applied voltage increases the electrostatic force between the membrane and the bottom electrode, hence, increasing the membrane deflection. Figure 2(a) plots the membrane deflection profiles for a range of applied biases from 0 to 20 V for a single cavity, showing a maximum center deflection of nearly $\Delta L = 60$ nm at 20 V. The increasing membrane deflection at higher voltages results in a decreasing optical cavity length, causing a blue-shift in optical emission.

Optical measurements were performed using a microscope setup to focus a $\lambda = 400$ nm pulsed excitation laser (1 kHz repetition rate, 100 fs pulse duration) through the

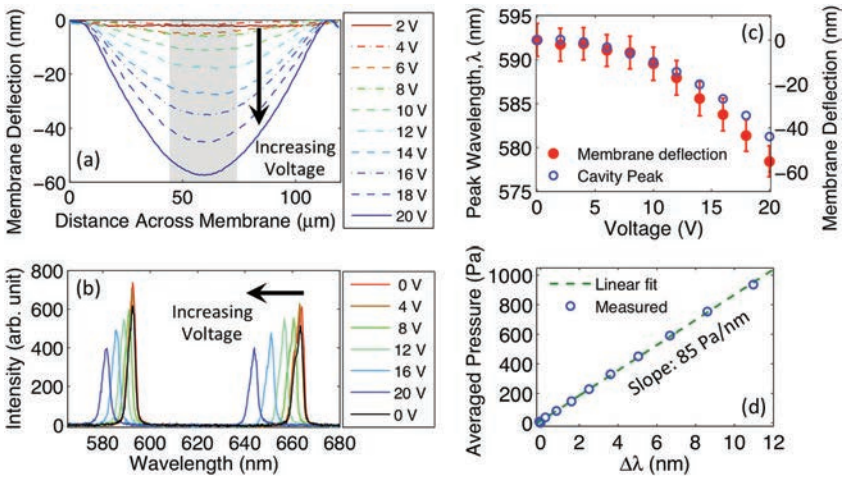

FIG. 2. (a) Height difference profile of a composite membrane under electrostatic actuation compared to 0 V, obtained via optical interferometry. Profiles show membrane deflection due to applied voltage for devices with a 1 μm-thick SU-8 layer. The shaded gray section indicates excitation spot size of $\sim$30 μm for emission measurements. (b) Device emission below lasing threshold demonstrating spectral shift in cavity modes under increasing applied voltage. A cavity mode spacing of 71 nm is observed, consistent with the 4λ cavity optical path length. (c) Shift in the $\lambda = 592$ nm cavity mode peak as a function of applied voltage bias (blue) obtained from cavity emission spectrum and average membrane profile obtained via interferometry. The error bars represent the standard deviation due to membrane roughness and membrane deflection variation within the illuminated excitation spot size. (d) Calculated average pressure across membrane due to applied bias compared to observed change in cavity emission peak wavelength. From a linear fit, the estimated pressure sensitivity for the 4λ cavity is 85 Pa/nm.

planar DBR into the cavity. The excitation wavelength is outside the DBR stopband, allowing for efficient excitation of the organic film. The same objective captures subsequent cavity mode emission, and the emission is focused into a grating spectrograph (Princeton Instruments Acton SP2300) with a charged-coupled device array detector (Princeton Instruments Pixis) for spectral analysis. In order to correlate cavity emission shift and membrane deflection, cavity emission spectra were collected with the same devices biased at the same actuation voltages as those used in the membrane deflection measurements. The optically pumped devices were tested in a nitrogen-rich environment at atmospheric pressure to minimize photo-oxidation damage to the organic gain medium.

A typical cavity mode luminescence emission spectrum of these MEMS VCSEL devices under a range of applied biases is plotted in Figure 2(b). As the applied bias increases from 0 V to 20 V, the cavity mode peak wavelengths shift by over 10 nm and reversibly return to their initial values when the voltage bias is removed. Since membrane curvature, and hence cavity length variation, increases with applied voltage, the cavity resonator experiences higher loss as evidenced by a slight decrease in peak intensity and increase in cavity mode width with increasing applied bias. The 30 μm excitation spot was centered to avoid the cavity edges where the top mirror exhibits the largest curvature, which would cause additional mode broadening and intensity loss. Figure 2(c) compares the shift in peak emission of the $\lambda = 592$ nm cavity mode (blue circles) and the corresponding change in membrane profile (red dots) for the same cavity, zeroed to the peak wavelength at 0 V. The error bars reflect a range of measured deflections due to membrane roughness and increased deflection curvature within the $\sim$30 μm excitation spot size at each applied voltage bias; the relatively consistent error bar lengths suggest that cavity length variation within the excitation spot is dominated by membrane roughness rather than deflection curvature. Given the calculated optical cavity length (4λ), peak wavelength shifts ($\Delta\lambda$) are expected to follow the relationship $4\Delta\lambda = \Delta L$, where ΔL is the change in air-gap spacing due to membrane deflection; the scales of the y-axes in Figure 2(c) reflect this relation. The average electrostatic pressure at each voltage is calculated using membrane deflections obtained via interferometry. Since both the membrane deflection and electrostatic pressure scale with the square of the applied voltage, the calculated pressure is proportional to the change in measured peak cavity emission, resulting in a device pressure sensitivity of 85 Pa/nm.

The second set of devices with a thinner, 570 nm-thick, SU-8 spacer layer was fabricated to reduce the actuation voltages and lasing threshold. Figure 3(a) plots the emission intensity of the 3λ device around the lasing threshold. Device lasing operation, demonstrated in Figure 3(b), shows a typical input-power-dependent emission intensity and spectral mode linewidth, computed using the full-width half-maximum. At pump powers over the lasing threshold of 200 μJ/cm^2 incident power, the observed cavity modes reduce to a single lasing mode with significantly increased peak intensity. Concurrently, the emission linewidth of the cavity mode reduces to that of the monochromic lasing mode.

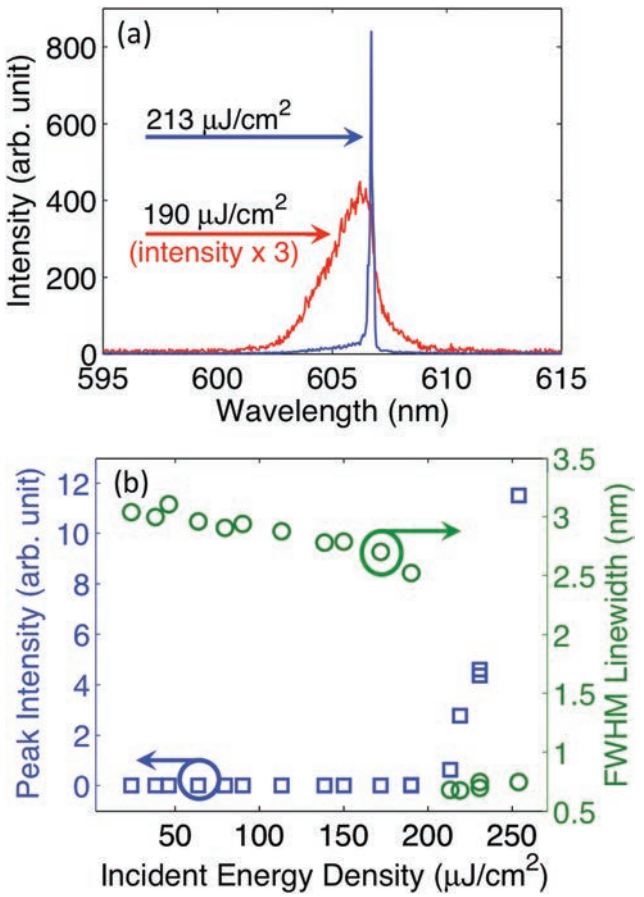

FIG. 3. (a) Device emission spectra for select pump energy densities to illustrate spectral output just below and just above the typical lasing threshold power. (b) Peak intensity of spectral mode (left axis) and mode width (right axis) as a function of estimated excitation energy density. Both the nonlinear increase in mode peak intensity and a sudden decrease in mode linewidth are indicative of a lasing threshold at 200 μJ/cm^2 incident power.

As previously observed for cavity modes in Figure 2, the lasing mode blue-shifts with electrostatic actuation of the composite membrane. For these shorter cavities, a $\Delta\lambda = 10$ nm laser mode shift occurs at a lower applied voltage of 6 V, as shown in Figure 4(a). The reversibility of the laser spectral shifts is highlighted in Figure 4(b). The laser emission hysteresis error is below 1 nm.

By varying the device geometry (e.g., spacer layer thickness, cavity diameter, and membrane thickness), the composite membrane-cavity structure demonstrated in this work can be optimized to enable spectral tuning over a wider range at low voltages, thus utilizing the full emission spectral range of the organic gain medium. One caveat is that the tunable range is limited by the need to avoid membrane pull-in and permanent stiction of the membrane to the cavity bottom. Membrane pull-in occurs in tunable electrostatic gaps when the attractive electrostatic force dominates the restoring elastic/spring force at larger deflections. Additionally, the oxygen-sensitivity of the Alq_3:DCM lasing medium and resulting photo-bleaching degradation limits device stability in non-inert environments, necessitating device encapsulation for stable, long-term device operation. Photo-oxidation of the organic gain medium can be observed in both spectral shift and intensity decrease over long periods of operation, resulting in loss of lasing modes. Although the laser can be

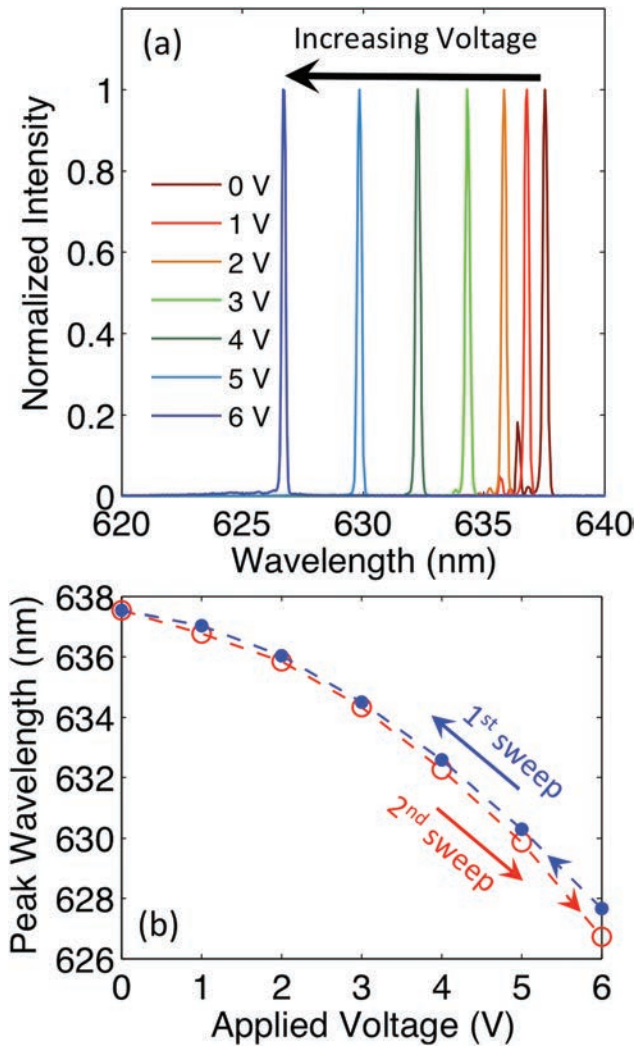

FIG. 4. (a) Tuning laser emission wavelength using electrostatic pressure, demonstrating reversible tunable range from $\lambda = 637$ nm to $\lambda = 628$ nm in response to 6 V actuation. (b) Peak wavelength of lasing mode as a function of applied bias, demonstrating less than 1 nm hysteresis between forward and reverse sweeps.

swept across a 10 nm range over repeated optical excitation tests, the observed gradual blue-shift of the tuning range by a few nanometers points to the need for device encapsulation or, alternatively, replacement of the Alq_3:DCM system with a more air-stable, flexible gain medium.

The demonstrated device structure may be directed beyond the tunable laser applications. Instead of electrostatically actuating the device membrane to tune the lasing frequency, the membrane can also be mechanically/pneumatically actuated to implement an optical, contactless-readout pressure sensor, where shifts in the cavity emission wavelength (above or below lasing threshold) are calibrated to indicate changes in pressure above the membrane. Assuming the same membrane deflection under equal mechanical pressures for both demonstrated device arrays, the estimated pressure sensitivity of the 4λ cavity in Figure 2(d) suggests a sensitivity of 64 Pa/nm for the thinner 3λ lasing device. The sensor response rate could potentially approach 2 MHz, as determined using a lumped-parameter force-deflection model and assuming no viscous-damping losses in the deflecting membrane. The pressure sensor sampling rate could also be limited by the lasing sampling rate above threshold; due to triplet loss mechanism in the organic gain medium, organic lasers often operate with repetition rates in the range of kHz.[15] However, this gain limitation can be circumvented by operating in cavity emission mode or by replacing the Alq_3:DCM with materials supporting continuous wave (CW) or quasi-CW lasing operation.

In conclusion, an electrostatically tunable organic MEMS VCSEL, enabled by a solvent-free additive membrane transfer fabrication technique, is demonstrated. Electrical actuation and optical characterization of a typical device show spectral tuning of $\Delta\lambda = 10$ nm at 6 V. Because the flexible composite membrane can be actuated either electrically or mechanically, these organic MEMS VCSEL structures can be applied to both tunable lasing in the visible or near-infrared range as well as all-optical, contactless, large area pressure-sensing applications.

The authors gratefully acknowledge funding from the National Science Foundation Center for Energy Efficient Electronics Science Award ECCS-0939514. G.M.A. acknowledges funding from the Hertz Foundation Graduate Fellowship. We also thank Parag Deotare for constructive discussions.

[1]V. G. Kozlov, V. Bulovic, P. E. Burrows, M. Baldo, V. B. Khalfin, G. Parthasarathy, S. R. Forrest, Y. You, and M. E. Thompson, J. Appl. Phys. **84**, 4096 (1998).
[2]I. D. W. Samuel and G. A. Turnbull, Chem. Rev. **107**, 1272 (2007).
[3]R. Brückner, M. Sudzius, H. Fröb, V. G. Lyssenko, and K. Leo, J. Appl. Phys. **109**, 103116 (2011).
[4]D. Schneider, T. Rabe, T. Riedl, T. Dobbertin, M. Kröger, E. Becker, H.-H. Johannes, W. Kowalsky, T. Weimann, J. Wang, and P. Hinze, Appl. Phys. Lett. **85**, 1886 (2004).
[5]A. Wang, W. Chang, A. Murarka, J. H. Lang, and V. Bulović, IEEE Int. Conf. Micro Electro Mech. Syst. **2014**, 1217.
[6]V. Bulović, V. G. Kozlov, V. B. Khalfin, and S. R. Forrest, Science **279**, 553 (1998).
[7]M. Zavelani-Rossi, G. Lanzani, S. De Silvestri, M. Anni, G. Gigli, R. Cingolani, G. Barbarella, and L. Favaretto, Appl. Phys. Lett. **79**, 4082 (2001).
[8]O. Mhibik, T. Leang, A. Siove, S. Forget, and S. Chénais, Appl. Phys. Lett. **102**, 041112 (2013).
[9]S. Döring, M. Kollosche, T. Rabe, J. Stumpe, and G. Kofod, Adv. Mater. **23**, 4265 (2011).
[10]S. Klinkhammer, N. Heussner, K. Huska, T. Bocksrocker, F. Geislhöringer, C. Vannahme, T. Mappes, and U. Lemmer, Appl. Phys. Lett. **99**, 023307 (2011).
[11]C. J. Chang-Hasnain, IEEE J. Sel. Top. Quantum Electron. **6**, 978 (2000).
[12]C. E. Packard, A. Murarka, E. W. Lam, M. A. Schmidt, and V. Bulović, Adv. Mater. **22**, 1840 (2010).
[13]R. Ozaki, Y. Matsuhisa, M. Ozaki, and K. Yoshino, Appl. Phys. Lett. **84**, 1844 (2004).
[14]V. G. Kozlov, V. Bulović, P. E. Burrows, and S. R. Forrest, Nature **389**, 362 (1997).
[15]Y. Zhang and S. R. Forrest, Phys. Rev. B **84**, 241301 (2011).